Core−Shell Polymer Nanoparticles for Baroplastic Processing

Juan A. Gonzalez-Leon, Sang-Woog Ryu, Sheldon A. Hewlett, Sarah H. Ibrahim, and Anne M. Mayes*

Department of Materials Science and Engineering, Massachusetts Institute of Technology, 77 Massachusetts Avenue, Cambridge, Massachusetts 02139

Received April 15, 2005; Revised Manuscript Received July 25, 2005

ABSTRACT: Core−shell polymer nanoparticles consisting of a low glass transition temperature (T_g) core of poly(*n*-butyl acrylate) or poly(2-ethylhexyl acrylate) and a glassy polystyrene shell were synthesized by two-stage emulsion polymerization. The obtained materials exhibit pressure-induced mixing of their components and could be processed at low temperatures (25−50 °C) by compression molding or extrusion. Nanoparticles of varying PS content and particle size were investigated to determine parametric effects on processing and mechanical properties. Transmission electron microscopy (TEM), differential scanning calorimetry (DSC), and small-angle neutron scattering (SANS) measurements performed before and after processing indicate the partial release of the soft component from the nanoparticle cores and subsequent intermixing with shells of adjacent particles under the application of pressure. The processed materials range from rigid plastics to elastomers with mechanical properties comparable to conventional styrenic thermoplastic elastomers (TPEs). Pressure-enhanced mixing is shown to play a crucial role in generating strong interfaces between the nanophase domains.

Introduction

With the development of styrenic block copolymers in the 1960s, thermoplastic elastomers (TPEs) were marketed as a convenient replacement for chemically cross-linked rubbers, providing better processability and recyclability.[1,2] In such materials, the glassy component domains function as physical cross-links, allowing the soft component to stretch and recover from applied stress. Commercial trade names of such TPEs include Stereon (Firestone), Kraton D (Kraton), and Septon (Kuraray) among others, which are polystyrene-*block*-polybutadiene-*block*-polystyrene (SBS) or polystyrene-*block*-poly(ethylene-*co*-butylene)-*block*-polystyrene (SEBS) block copolymers. Though not as heat and solvent resistant as cross-linked rubbers, TPE's have garnered a steadily increasing market over the past years, in applications such as footwear, wire insulation, hot melt adhesives, and sealants, reaching $1.8 billion in 2002.[3] The processing of TPEs encompasses the advantages and disadvantages of melt processing, including energy consumption associated with heating the TPE to form a melt and potential for thermal degradation. Currently, such materials are not recycled.[1,2]

As an alternative to hot melt processing, we recently reported the low-temperature processing of styrene/acrylic block copolymers, exploiting the pressure-induced miscibility of the low-T_g and high-T_g block components.[4] Such materials have been termed "baroplastics" for their ability to transform from a solid to a melt state via an order-to-disorder transition induced by applied pressure.[5−8] Though never fully disordering, baroplastic block copolymers of PS ($T_{g,PS}$ = 100 °C) and poly(butyl acrylate), PBA ($T_{g,PBA}$ = −50 °C), or poly(2-ethylhexyl acrylate), PEHA ($T_{g,PEHA}$ = −65 °C), were successfully compression-molded at room temperature under applied pressures of 34.5 MPa (5000 psi) for 5 min.[4]

It was further demonstrated that, like their block copolymer counterparts, core−shell polymer nanoparticles with (un-cross-linked) PBA or PEHA cores and PS shells can be molded and reprocessed at low temperatures in a semi-solid state to obtain solid, transparent objects.[4] Melt processing and solution casting of such systems are not viable because the two components will either macrophase separate or codissolve.[9] This discovery represents a departure from previous applications of core−shell nanoparticles as coatings[9−13] or impact strength modifiers for thermoplastics.[9,14]

The present work explores in more detail the structure−processing−property relationships of PBA/PS and PEHA/PS core−shell nanoparticle materials, examining the role of pressure enhanced miscibility, particle size, and particle composition on processing and the resultant mechanical properties. Core−shell materials are synthesized by a two-stage emulsion polymerization, rinsed, and vacuum-dried to obtain bulk powders for processing studies. Transmission electron microscopy (TEM), differential scanning calorimetry (DSC), and small-angle neutron scattering (SANS) techniques are used to probe the morphology and structure before and after processing by compression molding or extrusion. The processed materials range from rigid plastics for systems of higher PS content (∼60 wt %) to elastomers akin to styrenic block copolymer TPEs for PS contents ∼40 wt %. To address the role of pressure-enhanced mixing, a control was prepared having a PS shell and poly(lauryl methacrylate), PLMA ($T_{g,PLMA}$ = −55 °C), core. Despite the tendency for this system to demix upon the application of pressure,[8] PS/PLMA nanoparticles could also be processed at low temperature; however, the processed product exhibits poor tear strength, attributable to the weak interface between PS and PLMA nanodomains.

Experimental Methodology

Materials. Styrene (S, 99%), 2-ethylhexyl acrylate (EHA, 99%), *n*-butyl acrylate (BA, 99%), and *n*-lauryl methacrylate (LMA, 96%) were purchased from Aldrich. Deuterated styrene (d8-S, 98%) was purchased from Cambridge Isotope Laboratories. Inhibitors were removed from the monomers prior to polymerization by passing through a column packed with basic aluminum oxide (Aldrich). Tetradecyltrimethylammonium

10.1021/ma0508045 CCC: $30.25
Published on Web 08/24/2005

Table 1. Size and Composition of Core−Shell Nanoparticles and Block Copolymers

core/shell	composition[a] (PS wt %)	particle size (nm)[b] core/core−shell	particle size (nm)[c] (calcd) core−shell	M_w/M_n (g/mol) core	M_w/M_n (g/mol) shell
BS1 PBA_{43}/PS_{57}	57	163/201	215	561K/190K	48K/4K
BS2 PBA_{37}/PS_{63}	63	49/62	68	480K/156K	256K/112K
BS3 PBA_{34}/d8-PS_{67}	67 (calcd)	59/82	85	707K/64K	654K/71K
BS4 PBA_{47}/PS_{53}	53	65 (shell)		2×10^6 [d]/1.53×10^6	1.2×10^6/153K
BS5 PBA_{56}/PS_{44}	44	55/58	67	167K/68K	1.0×10^6/400K
BS6 PBA_{59}/PS_{41}	41	55/60	65	991K/346K	133K/10K
BS7 PBA_{42}/PS_{58}	58	43/53	57	736K/129K	56K/7K
BS8 PBA_{37}/PS_{63}	63	61/78	85	994K/324K	27K/3K
BS9 PBA_{36}/PS_{64}	64	102/154	143	852K/230K	99K/9K
BS10 PBA_{49}/PS_{51}	51	58/72	73	622K/141K	190K/45K
BS11 PBA_{51}/PS_{49}	49	50/60	62	657K/35K	18K/4K
ES1 $PEHA_{51}/PS_{49}$	49	61/74	76	1.1×10^6/495K	910K/303K
ES2 $PEHA_{42}/PS_{58}$	58	60/75	80	1.28×10^6/443K	1.1×10^6/473K
ES3 $PEHA_{62}/PS_{38}$	38	64/70	75	1.18×10^6/149K	84K/8.5K
ES4 $PEHA_{61}/PS_{39}$	39	58/72	68	469K/76K	1.1×10^6/890K
LS1 PLMA/PS	54	59/61	76	1.1×10^6/518K	222K/127K
SB PS-*b*-PB	30			96K/90K	
SIS PS-*b*-PI-*b*-PS	22			135K/110K	

[a] Calculated by ^{1}H NMR. [b] Measured by dynamic light scattering. [c] Calculated from ^{1}H NMR and eq 1. [d] Outside GPC calibration limit.

bromide (TTAB, 99%, Aldrich), 2,2′-azobis(2-methylpropionamidine) dihydrochloride (V50, 97%, Aldrich), 1-dodecanethiol (DT, 98%, Aldrich), and acetone (97%, J.T. Baker) were used without further purification. Deionized (DI) water was used throughout the experiments. Polystyrene-*block*-polyisoprene-*block*-polystyrene (SIS) and polystyrene-*block*-polybutadiene (SB) block copolymers were purchased from Aldrich and used as received.

Polymerization Procedure. Core−shell nanoparticles were synthesized by a two-stage emulsion polymerization technique as reported by Ha et al.[15] In a typical procedure, under a N_2 atmosphere, 60 g of water, emulsifier (TTAB, 0.9 g, 12 mmol), and acetone (7 g, 30 mmol) were added to a 250 mL glass reactor prewashed with 1 N HCl solution and DI water. After purging with N_2 for 30 min, the solution was heated to 65 °C under vigorous stirring. EHA (9 g, 20 mmol) or BA was then added slowly, over approximately a half hour period, and stirred for an extra 1 h. The first-stage emulsion polymerization was initiated by the addition of V50 (0.1 g, 1 mmol) and allowed to proceed for 15 h. In the second stage, preemulsified styrene (9 g, 20 mmol) using 75 g of water, acetone (7 g, 30 mmol), and chain transfer agent (DT, 0.2 g, 1 mmol) was then added slowly to the reactor (addition rate: 0.09 g/min) using a cannular syringe equipped with a nitrogen pressure pump. After 13 h of reaction time, prepared emulsions were poured into excess methanol/water mixtures (5/1, v/v, containing trace amounts of NaCl) causing the core−shell particles to precipitate. To remove residual emulsifier, the obtained product was washed several times with a mixture of deionized water and methanol and then dried in a vacuum oven for 3 days at room temperature in the presence of phosphorus pentoxide. A control sample incorporating a PLMA core and a PS shell was also synthesized following a similar procedure as described above. Samples with a lower molecular weight core polymer were obtained by adding chain transfer agent (0.2 g) in the first stage of the polymerization.

To study the kinetics of particle growth, samples were extracted from the reaction vessel at varying reaction times during synthesis of a PEHA/PS system and quenched immediately with hydroquinone to prevent further polymerization. Quenching is required since it is known that the reaction rate in emulsion polymerization is fast due to the reduced possibility of termination between two radicals inside a micelle.[16] For this polymerization, 12 wt % of emulsifier, 0.01 wt % of initiator (based on the amount of EHA), and a feed rate of the styrene monomer in the second stage of 0.09 g/min were used.

Characterization. The particle size distribution was determined at 25 °C in deionized water using a ZetaPALS particle sizer (Brookhaven Instruments Co.) fitted with a 676 nm laser source. ^{1}H nuclear magnetic resonance (NMR) spectra were recorded on a Bruker DPX (300 MHz) by dissolving the particles in $CDCl_3$. Gel permeation chromatography (GPC) was performed at 25 °C on a Viscotek GPCmax instrument equipped with refractive index and ultraviolet detectors to obtain the molecular weight relative to polystyrene standards. THF was the eluent at a flow rate of 1.0 mL/min. Glass transition temperatures were measured with a Q100 TA Instruments differential scanning calorimeter (DSC) at a scan rate of 20 °C/min.

Transmission electron microscopy was carried out on a JEOL 200CX TEM, operated at 160 kV. Samples were cryomicrotomed in a MT-X ultramicrotome set to 25 nm. Specimens were subsequently stained with RuO_4 for 20 min. Small-angle neutron scattering (SANS) was measured at the Manuel Lujan Jr. Neutron Scattering Center at Los Alamos National Laboratory on the Low-Q diffractometer, LQD, with the following instrument configuration: wavelength = 1.5−15 Å at 20 Hz, scattering angle = 6−60 mrad on a 59 cm diameter detector, resulting in a q range of 0.003−0.5 Å^{-1}. Samples were ~1 cm diameter disks of variable thickness. Scattered intensities were corrected for background and thickness in the standard manner.

Samples were processed on a Grimco hydraulic press with temperature control and on a Carver Inc. Auto Series press with a force controlled unit using custom-made aluminum and stainless steel molds. Dogbone-shaped samples were cut from films obtained either by extrusion from a custom-made piston mold or by compression molding between two plates employing a ~0.5 mm thick spacer. Tensile tests and tear strength measurements were carried out using an Instron 4501 at a rate of 30 mm/min under ambient conditions. At least two specimens were measured for each sample. Engineering stress is reported in every case.

Results and Discussion

Particle Synthesis and Characterization. Table 1 lists the characteristics of core−shell nanoparticle systems synthesized by two-stage emulsion polymerization. Compositions of the resulting particles ranged from 38 to 67 wt % PS, as calculated from the integral ratio of characteristic resonances for PS at 6.3−7.2 ppm (styrene aromatic) and the core polymer at 3.9−4.1 ppm (−OCH_2− of BA or EHA) from ^{1}H NMR measurement. ^{13}C NMR measurements were also performed to check for branching or cross-linking of the acrylate components.[17] No branching was observed to within the instrument resolution. However, high molecular weights

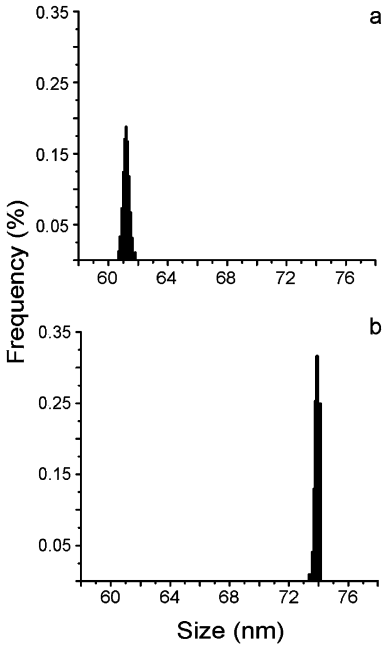

Figure 1. Particle size distribution histograms of (a) PEHA core and (b) $PEHA_{51}/PS_{49}$ (ES1) core−shell.

for the acrylates and methacrylates were obtained. The molecular weights were poorly controlled, and GPC traces show that the core and the shell polymers both exhibit very large polydispersities (PDI range ∼2−10, Table 1). Core sizes obtained during the first stage of polymerization ranged between 43 and 163 nm, as determined by dynamic light scattering (DLS). Average particle size increased after adding the styrene monomer in the second stage. Final particle sizes in the range of 50−200 nm in diameter were obtained. Table 1 also shows particle diameters predicted from compositions obtained by NMR using the following geometrical relation:

$$D_{c-s} = D_c\left(1 + \frac{M_s}{\rho_s}\frac{\rho_c}{M_c}\right)^{1/3} \quad (1)$$

where D_c and D_{c-s} are the diameter of the core and final core−shell particles, respectively, and M_i and ρ_i are the mass fraction and mass density of component i (core or shell). The obtained diameter values are close to those from DLS. The differences observed may be attributed to inaccuracy in the densities employed in calculating eq 1 ($\rho_s = 1.06$ g/cm^3, $\rho_c = 1.07$ g/cm^3).

Figure 1 shows representative particle size distribution histograms of the parent PEHA core and final $PEHA_{51}/PS_{49}$ (ES1) core−shell particles. Both histograms indicate very narrow particle size distributions.[18] Results of kinetics studies on a PEHA/PS system (Figure 2) show that the average particle size increased monotonically in the first 3 h of stage one and then remained almost constant for 11 h, indicating that the EHA was effectively consumed. Particle size increased with the addition of styrene and reached 80 nm with no evidence of residual core particles, although the rate of particle growth in the second stage was slightly lower.

Coverage of the poly(acrylate) core by the polystyrene shell appears complete for higher PS content samples (above 50 wt % PS), for which a powdery product is obtained upon precipitation. Figure 3 shows a TEM micrograph of cryomicrotomed PBA_{43}/PS_{57} particles

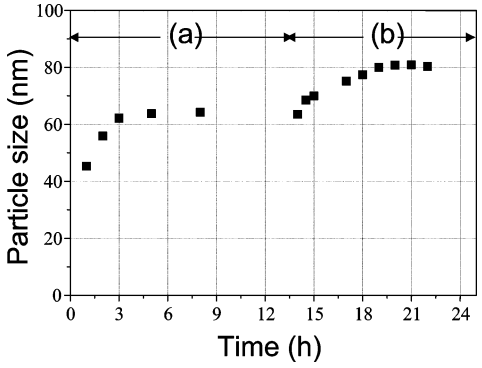

Figure 2. Particle size evolution of (a) first and (b) second stage as a function of polymerization time for a $PEHA_{51}/PS_{49}$ (ES1) system at 65 °C.

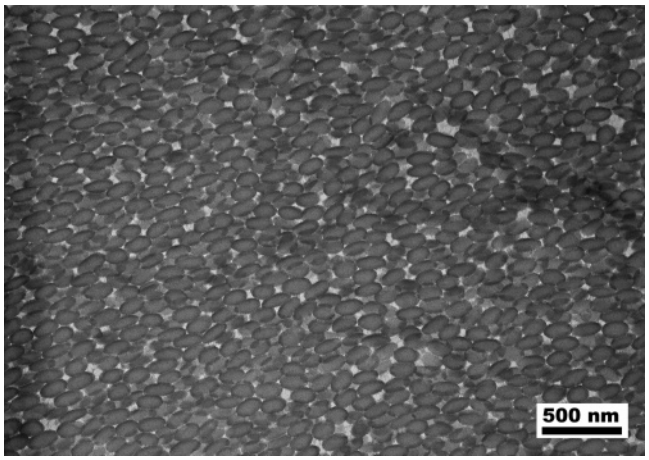

Figure 3. TEM image from PBA_{43}/PS_{57} (BS1) processed at 25 °C under 34.5 MPa for 5 min.

(BS1) after processing, where the core−shell structure can be clearly observed. In this image, the PBA core is surrounded by a dark PS shell, which is selectively stained by RuO_4.[14] Interestingly, the observed particles are not spherical but ellipsoidal and directionally oriented. These structural features are likely due to uniaxial deformation occurring during sample preparation, since AFM images of the particles dried from the emulsion state revealed them to be spherical in shape.

Further analysis of the nanoparticle structure was conducted by modulated differential scanning calorimetry (MDSC). Figure 4 shows a typical MDSC heat flow curve for the core−shell nanoparticles as dried. Two distinct glass transitions are observed as expected in a microphase-separated structure. In addition, a mixed glass transition, $T_{g,mix}$, is observed around 60 °C, which is attributed to the interphase of the two components. Through careful measurement of the changes in specific heat (ΔC_p) at each component's glass transition, it is possible to quantify the amount of each component at the interphase.[19−21] The analysis yielded that about half of the polystyrene homopolymer is mixed with core homopolymer, which results in interphases on the order of 3−5 nm thick, with average compositions in the range 70−90 wt % PS. Composition values were also calculated using the measured $T_{g,mix}$ from MDSC through the Fox equation. The obtained compositions are in good agreement with those determined from ΔC_p measurements. In some cases, the interphase size nearly matches the calculated PS shell thickness, consistent with TEM micrographs of the corresponding samples, where only

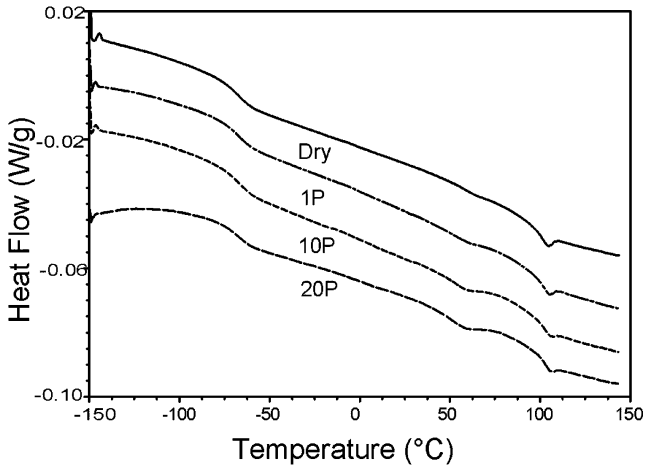

Figure 4. MDSC measurements of $PEHA_{42}/PS_{58}$ (ES2) as-dried and processed 1 (1P), 10 (10P), and 20 (20P) times at 25 °C using the piston mold.

Figure 5. Processed samples of PBA_{37}/PS_{63} (BS2) at 25 °C under 34.5 MPa for 1 min. Middle box contains original dry powder as obtained from polymerization.

a thin PS shell was observed. For lower PS contents, the obtained samples were not as powdery, which might indicate incomplete coverage of the core by the glassy shell component.[19,22]

Processability of Baroplastic Nanoparticles. As recently demonstrated, core−shell nanoparticles prepared with PS shells and PBA or PEHA cores can be processed by compression molding at temperatures as low as room temperature.[4] For example, Figure 5 shows compression-molded lids of PBA_{37}/PS_{63} (BS2) processed at an applied pressure of 34.5 MPa, for 1 min at 25 °C along with the dry raw material as obtained from the polymerization. It has been previously reported that PBA and PS exhibit pressure-induced mixing; i.e., when pressure is applied, the two components become more miscible, with the low-T_g component acting as a "solvent" for the glassy component at low temperatures.[4] Figure 6 shows SANS evidence of such mixing in a deuterated sample of PBA_{34}/d8-PS_{67} nanoparticles (BS3) after applying 34.5 MPa of compression for different times at 25 °C. The intensity of the scattering peak at $q \sim 0.085$ nm^{-1} ($d \sim 74$ nm) decreases with increasing processing time, indicating lower contrast between PS and PBA domains consistent with increased mixing. Nevertheless, the peak persists even after 30 min of applied pressure, suggesting that distinct domains of

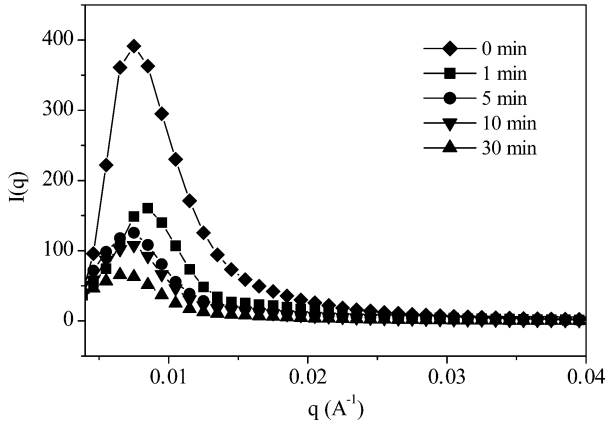

Figure 6. Scattering intensity profile as a function of processing time at 25 °C under 34.5 MPa for PBA_{34}/d8-PS_{67} (BS3).

PS and PBA remain in the sample. The peak position is also observed to shift under pressure. After short processing times (1 min), a shift is seen to larger wavevector, consistent with densification of the powder, as observed previously.[4] At longer times the peak shifts to lower wavevectors, indicating an increase in the characteristic period of the nanophase structure. This is thought to be due to deformation of the domains during processing, leading to larger domain sizes in the direction normal to the applied force. DSC first heat measurements of the same material after 1, 10, and 30 min under pressure show in every case both components' T_g's, confirming the partial retention of the two phases, along with an increasing signature from a mixed-phase T_g around 47 °C with increased processing time.

The presence of distinct domains after processing suggests that the application of pressure creates a mobile PBA layer around portions of the glassy PS component that facilitates flow of the entire system and gives cohesion to the processed product. An analogous phenomenon has been reported previously for chocolate processing,[23] wherein well-defined extrudates were obtained ~10 deg below the melting point. The soft, cocoa butter component apparently mobilizes the unmelted sugar crystals (which comprise about 45% of the mixture) and other solid components under sufficient applied pressure.

A key question, then, is what role does pressure-induced miscibility play on the processing and properties of core−shell nanoparticles? To address this issue, a core−shell material with a poly(lauryl methacrylate) (PLMA) core ($T_g \sim -55$ °C) and PS shell was synthesized (LS1). Though PLMA has a T_g comparable to that of PBA and PEHA, it exhibits an increased tendency to *demix* from PS when placed under pressure,[8] providing a useful control for examining the role of pressure-enhanced mixing. Notably, PLMA/PS nanoparticles of comparable acrylate molecular weight, soft to hard component ratio, and size to the PBA_{47}/PS_{53} (BS4) material could similarly be processed at reduced temperatures from the powdery precipitate. These findings demonstrate, as might be suspected from other (non-polymer) examples of semisolid processing,[24] that flow at reduced temperatures is not unique to core−shell systems that show pressure-induced mixing but is highly dependent on the soft to hard component ratio. However, as described in more detail below, the mechanical properties of this system were far inferior to

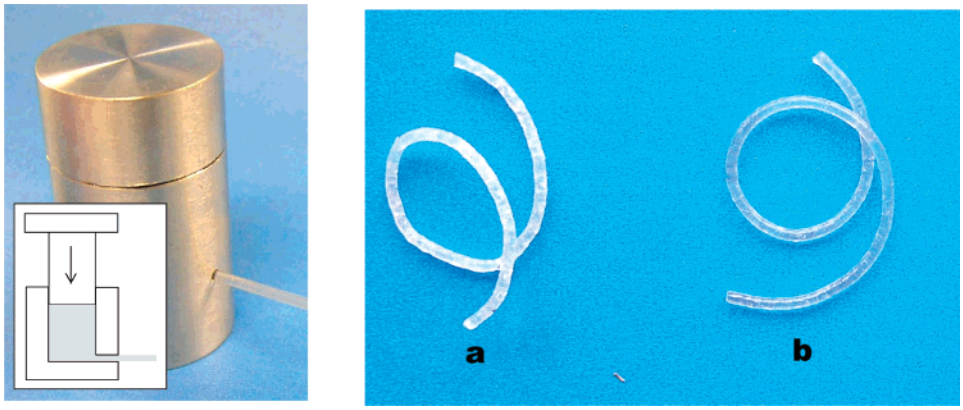

Figure 7. Piston mold and extrudates of $PEHA_{42}/PS_{58}$ (ES2) processed (a) 1 time and (b) 10 times at 25 °C.

BS4, particularly the tear strength. Indeed, SANS measurements on processed PLMA/PS samples showed an increase in peak intensity with increased processing time, opposite to the results seen in Figure 6, supporting the notion that pressure weakens the interface between these components through demixing.

As shown previously, core−shell nanoparticles can be remolded under compression multiple times at low temperatures.[4] However, a strong dependence on the composition is observed for the processing. By simple compression molding, well-defined objects were generally obtained at room temperature when starting from the powdery precipitate in a PS composition range from ~45 to 65 wt %. For lower PS contents, the highly elastic nature of the material led to shrinkage after processing. In most cases a processing temperature of 50 °C was sufficient to obtain a nondeformed sample from these systems. Similarly, processing temperatures of 40−50 °C were generally required for satisfactory processing and remolding of systems with PS contents above ~65 wt %. In both cases, the improved processing at elevated temperature may be attributable to enhanced mobility of the interphase.

To test the possibility of processing core−shell nanoparticles by extrusion, a custom-made "extrusion piston" was fabricated, comprising a two-part mold consisting of a piston and a chamber with a small orifice (0.5 mm diameter) on one side from which the polymer can flow when subjected to pressure from the piston (Figure 7). This simple geometry enables calculation of the true pressure applied to the material to allow an estimate of the material viscosity. The length-to-diameter ratio of the piston mold (L/D) is similar to a capillary viscometer.[25] A first approximation of the apparent viscosity, η_{app}, can be calculated using the simple solution for Poiseuille flow through a cylindrical channel of known dimensions:

$$\eta_{app} = \frac{\pi \Delta P D^4}{128 Q L} \tag{2}$$

where Q is the mass flow rate and ΔP is the difference between the pressure applied and the outlet pressure (in our case atmospheric pressure). Figure 8 shows the obtained apparent viscosity for the $PEHA_{51}/PS_{49}$ system (ES1) as a function of the shear rate at the wall ($\dot{\gamma}$) calculated as

$$\dot{\gamma} = \frac{32Q}{\pi D^3} \tag{3}$$

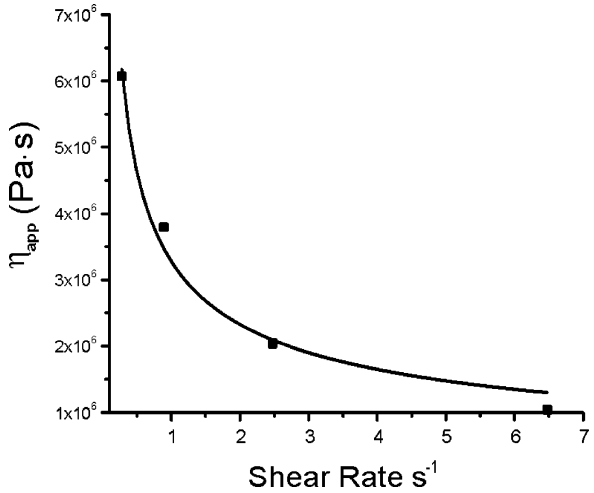

Figure 8. Apparent viscosity of $PEHA_{51}/PS_{49}$ (ES1) at 25 °C as a function of the applied shear rate: (■) experimental points; (- - -) power law fit.

The estimated viscosities through this simple calculation, $\eta_{app} \sim (1-6) \times 10^6$ Pa·s, are in the neighborhood of that of working glass, in the higher range of polymer processing, and, perhaps fortuitously, on the same order as those for chocolate cold extrusion.[23−25] From the dependence of viscosity on shear rate, the extruded material behaves as a pseudoplastic fluid, exhibiting a power law dependence on $\dot{\gamma}$ of the form[25]

$$\eta = \eta_0 \dot{\gamma}^{n-1} \tag{4}$$

where η_0 has a value of 3.27×10^6 Pa·s and n is equal to 0.503.

Changes in the rheological behavior could also occur by chain scission during processing. To examine this possibility, GPC measurements were performed on ES2 as-dried and after 10 and 20 extrusion cycles. UV detection at 254 nm was used to identify PS peaks from the refractive index (RI) signal that incorporates the sum of the two components. Individual molecular weight distributions were fit from the collected data. As shown in Figure 9, the PEHA distribution shifts toward lower molecular weights as a function of the number of processing cycles. The raw material PEHA has a M_w of about 1.28×10^6 g/mol, compared with 595 kg/mol after 10 extrusion cycles and 465 kg/mol after 20 cycles. This is not surprising since shear scission of very large chains ($>10^6$ g/mol) during flow through small channels has been reported previously.[26] It is also typical that such chain scission occurs near the middle of the chain,[27−29]

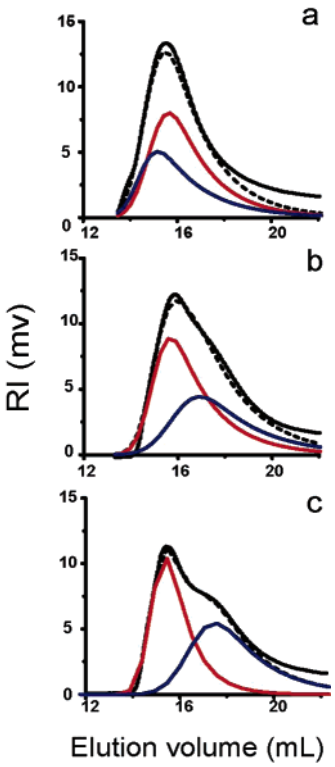

Figure 9. GPC traces for $PEHA_{42}/PS_{58}$ (ES2): (a) as-dried and processed (b) 10 times and (c) 20 times at 25 °C with piston mold. Fitted molecular weight distributions for PEHA (blue) and PS (red) shown.

as observed in the present system. The PS chains, by contrast, retain a M_w of 1.1×10^6 kg/mol. The same experiment was performed on a lower core molecular weight sample, PBA_{56}/PS_{44} (BS5). In this case no evidence of chain scission for either component was observed after processing.

Materials processed by extrusion exhibited facile room temperature recycling, even for systems with higher PS content. Figure 7 shows the piston mold extrudates of $PEHA_{42}/PS_{58}$ (ES2) after 1 and 10 processing cycles under a pressure of 207 MPa (27 kN applied) at 25 °C. For each cycle, the extrudate was chopped into ~2 mm pieces and reintroduced into the piston chamber for reprocessing. A more uniform extrudate is obtained with increasing processing steps beginning from the powder, consistent with the higher degree of mixing shown by SANS and DSC with increased processing time. Figure 4 compares MDSC measurements for the $PEHA_{42}/PS_{58}$ (ES2) core−shell dry powder with the same material after 10 and 20 processing cycles. In all cases the PEHA and PS T_g's are present, indicating distinct hard and soft microdomains; in addition, the mixed phase T_g is always present around 60 °C, which increases in signal with the number of processing cycles.

Figure 10a,b shows TEM images of ES2 as precipitated and after 20 cycles at 25 °C using a pressure of 207 MPa. After 20 processing operations, the core−shell structure is still clearly visible. Points where two adjacent core−shell particles break and combine can also be seen, consistent with the flow mechanism proposed for these materials. The axial deformation of the core−shell particles observed in the TEM images is most probably due to the microtoming process, since cuts were made perpendicular to the direction of flow.[30] Apparently, cohesion is achieved by the release of the low-T_g component from the core under pressure to serve as a "binder" between the core−shell particles and provide a mobile matrix. In this proposed mechanism, the mobile low-T_g component would be the one subjected to shear, carrying the largely intact PS domains during processing. This would explain why the PS molecular weight distribution is conserved after multiple recycles.

Mechanical Properties. Tensile tests were carried out on core−shell baroplastics as well as on commercial block copolymer TPEs. The results are summarized in Table 2. A diverse range of mechanical properties can be achieved depending on the low-T_g to high-T_g component ratio. Figure 11 shows stress−strain curves for three PBA/PS nanoparticle systems of different compositions that were processed by compression molding at 50 °C with an applied pressure of 34.5 MPa for 5 min (curves a−c). The mechanical properties are found to be highly sensitive to composition, with moduli and strains to break ranging from 209 MPa and 400% for a material with 58 wt % PS (curve a) to 13 MPa and 1200% for a system with 41 wt % PS (curve c). Curves d and e of Figure 11 show for comparison the stress−strain curves of SIS (curve d) and SB (curve e) commercial block copolymers processed by compression molding at 130 °C. The core−shell systems exhibit higher yield stresses and moduli than the styrenic block copolymer TPEs, but somewhat lower strain to break.

The tensile set was additionally measured for lower PS content core−shell materials PBA_{59}/PS_{41} (BS6) and $PEHA_{62}/PS_{38}$ (ES3) to compare with the block copolymer TPEs. The tensile set is a measure of the recovery capability of the material after a 100% strain for a specified time (10 min). The reported number is the percentage of permanent deformation after the test. For PBA_{59}/PS_{41} (BS6) and $PEHA_{62}/PS_{38}$ (ES3), the tensile set values are 23% and 10%, respectively, similar to the SB diblock value (9%), but substantially higher than the SIS triblock (3%).[31]

The effect of particle size on the mechanical behavior of core−shell materials was also studied. Figure 12 compares the stress−strain curves for PBA_{42}/PS_{58} (BS7), having an average diameter of 53 nm, and PBA_{43}/PS_{57} (BS1), with 201 nm average diameter. Interestingly, the larger particles do not exhibit the yielding peak notable for the smaller diameter sample. In addition, a substantial reduction in modulus occurs, from 180 MPa for the smaller nanoparticles (curve a) to 26 MPa for the larger ones (curve b). For higher PS contents, a similar size effect was observed comparing the PBA_{37}/PS_{63} (BS8) system having an average diameter of 78 nm with the larger PBA_{36}/PS_{64} (BS9) system having 154 nm diameter particles. In this case, the change in Young's modulus, from 199 to 64 MPa, is coupled to a substantial decrease in strain to break, as can be observed from curves c and d in Figure 12 (bottom).

For core−shell baroplastics, the nanoparticle diameter establishes the domain size of each component and, perhaps more importantly, the amount of surface area between them. As the domain size becomes larger, the soft component becomes less efficient as a toughener.

For example, melt mixed blends of PS and PB, in a comparable composition range to our materials, form domain sizes of ~2 μm, which lead to low Young's modulus (below 25 MPa), and elongations at break below 80%.[32] Because core−shell baroplastic components intermix under pressure to achieve cohesion, the larger the surface area per volume between the two

Table 2. Mechanical Properties of Core−Shell Nanoparticles and Block Copolymers

core/shell[a]	no. of samples	Young's modulus (MPa)	yield strength (MPa)	strain to break (%)	strength at break (MPa)
BS1 PBA_{43}/PS_{57}	3	26 ± 14		202 ± 31	2.6 ± 0.6
BS4 PBA_{47}/PS_{53}	2	110 ± 1.84	2.3 ± 0.21	945 ± 10.61	4.66 ± 0.11
BS5 PBA_{56}/PS_{44}	7	12.40 ± 1.9	0.40 ± 0.02	182 ± 68	0.14 ± 0.04
BS6 (50 °C) PBA_{59}/PS_{41}	3	13 ± 4	0.6 ± 0.1	outside range (>1100%)	at 1000% 1.2 ± 0.33
BS7 PBA_{42}/PS_{58}	3	180 ± 39	4.28 ± 0.07	134 ± 26	3.2 ± 0.2
BS7 (50 °C) PBA_{42}/PS_{58}	4	215 ± 15	4.92 ± 0.22	146 ± 124	4.3 ± 0.8
BS8 PBA_{37}/PS_{63}	3	199 ± 14	4.85 ± 0.4	210 ± 31	5.2 ± 1.1
BS9 PBA_{36}/PS_{64}	4	64 ± 6.8	2.8 ± 0.1	81 ± 6	1.5 ± 0.3
BS10 PBA_{49}/PS_{51}	3	96 ± 8.6	2.1 ± 0.1	664 ± 36.6	3.5 ± 0.2
BS11 PBA_{51}/PS_{49}	3	50 ± 5	1.2 ± 0.1	911 ± 92	1.9 ± 0.1
BS11 (50 °C) PBA_{51}/PS_{49}	3	78 ± 24	1.9 ± 0.2	1132 ± 14	2.7 ± 0.4
ES1 (50 °C) $PEHA_{51}/PS_{49}$	2	180 ± 39	0.5 ± 0.05	914 ± 93	1.5 ± 0.1
ES2 (50 °C) $PEHA_{42}/PS_{58}$	2	77 ± 7.8	1.9 ± 0.1	678 ± 34	2.9 ± 0.2
ES3 (50 °C) $PEHA_{62}/PS_{38}$	11	3.8 ± 1.8		486 ± 140	0.64 ± 0.5
ES4 (50 °C) $PEHA_{61}/PS_{39}$	3	3.5 ± 1		218 ± 48	0.1 ± 0.02
LS1 PLMA/PS	3	59.87 ± 8.39	1.82 ± 0.06	239 ± 33.87	2.23 ± 0.36
PS-*b*-PB (130 °C)	2	13 ± 3	0.8 ± 0.04	outside range (>1100%)	at 1000% 1.2 ± 0.1
PS-*b*-PI-*b*-PS (130 °C)	3	1 ± 0.4		outside range (>1100%)	at 1000% 4.5 ± 0.3

[a] Samples processed at 25 °C unless noted.

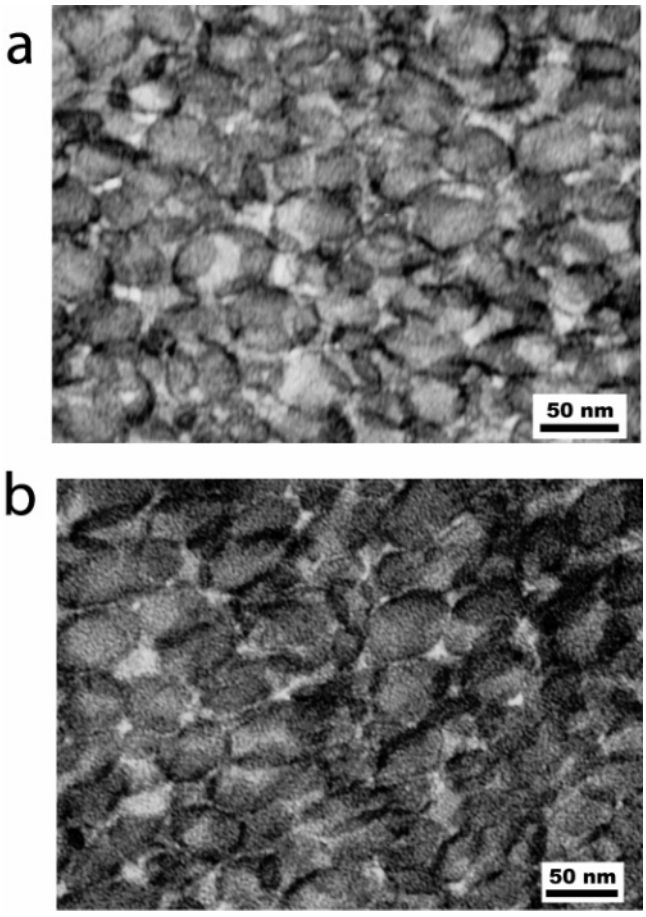

Figure 10. TEM image from $PEHA_{42}/PS_{58}$ (ES2): (a) as-dried and (b) processed 20 times at 25 °C.

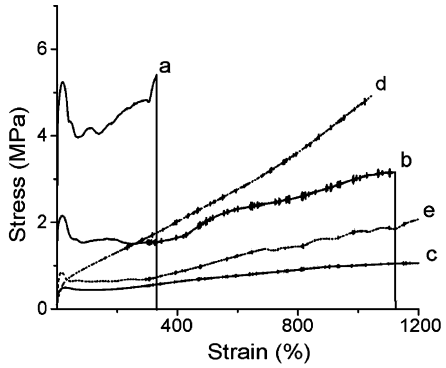

Figure 11. Stress vs strain curve for the core−shell baroplastics: (a) PBA_{42}/PS_{58} (BS7), (b) PBA_{51}/PS_{49} (BS11), (c) PBA_{59}/PS_{41} (BS6) and commercial TPEs, (d) SIS, and (e) SB.

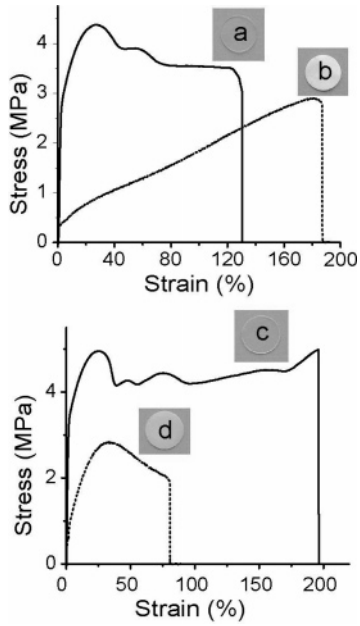

Figure 12. Stress vs strain curves and processed films for (a) PBA_{42}/PS_{58} (BS7) and (b) PBA_{43}/PS_{57} (BS1) molded at 25 °C under 34.5 MPa for 5 min, (c) PBA_{37}/PS_{63} (BS8), and (d) PBA_{36}/PS_{64} (BS9) molded at 35 °C under 34.5 MPa for 5 min.

domains, the better the mechanical properties of the processed form. For larger particles, the retention of distinct hard and soft domains after processing is further manifested in their transparent or opaque optical properties after molding (Figure 12 insets).

To understand the effect of the core polymer molecular weight on the mechanical properties, samples with lower acrylate molecular weight but similar size and polystyrene content were prepared. As shown in Table 2, the lower acrylate molecular weight BS5 and ES4 systems exhibit a lower strain to break and correspondingly a lower strength at break than the higher molecular weight BS6 and ES3. However, the modulus and yield strength are similar, even though the PS molecular

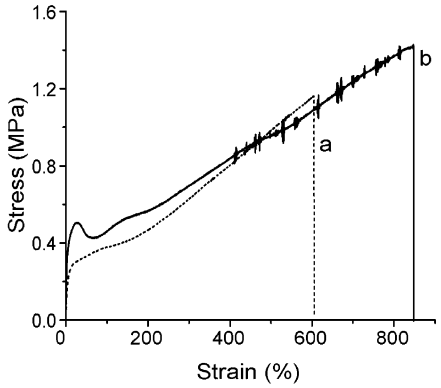

Figure 13. Stress vs strain curve for $PEHA_{51}/PS_{49}$ (ES1) processed at 34.5 MPa for 5 min at (a) 25 and (b) 50 °C.

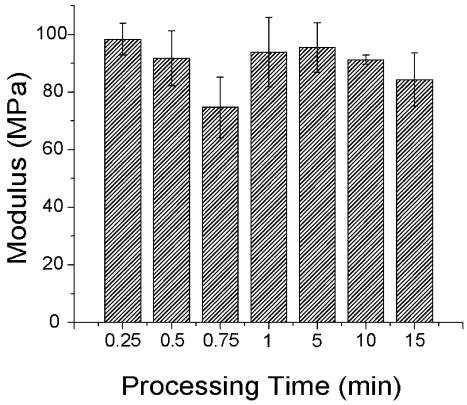

Figure 14. Modulus values for PBA_{49}/PS_{51} (BS10) samples processed at 25 °C under 34.5 MPa for different times.

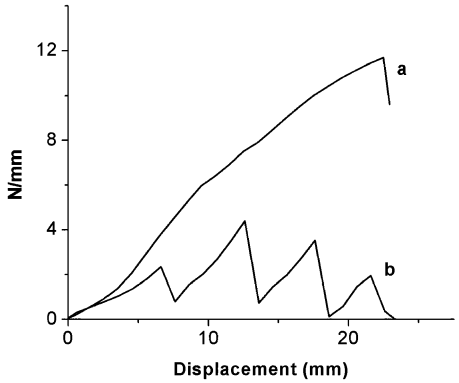

Figure 15. Force/sample thickness vs displacement plot from tear strength test for (a) PBA_{47}/PS_{53} (BS4) and (b) $PLMA_{46}/PS_{54}$ (LS1) processed at 25 °C under 34.5 MPa for 5 min.

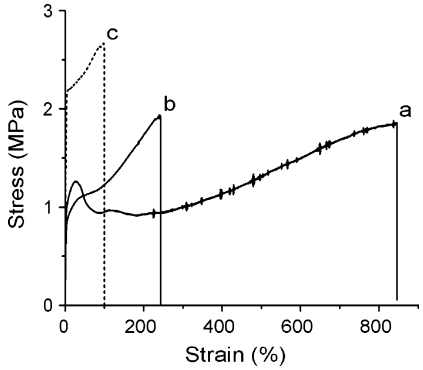

Figure 16. Stress vs strain curves for PBA_{51}/PS_{49} (BS11): (a) processed by compression molding at 25 °C under 34.5 MPa for 5 min and processed with the piston mold (b) 1 time and (c) 10 times at 25 °C.

weight is lower in the higher molecular weight acrylate samples. This suggests that the modulus and yield strength depend more on the PS content than on its molecular weight for these core−shell materials. It also indicates that the strain to break and ultimate strength might depend heavily on the molecular weight of the acrylate, which works as a carrier and binder for the PS domains.

Processing temperature also affects the final mechanical properties of the core−shell materials. Figure 13 shows stress−strain plots for $PEHA_{51}/PS_{49}$ (ES1) processed at 25 and 50 °C by compression molding under an applied pressure of 34.5 MPa for 5 min. Processing 25 deg above room temperature increases the modulus from 10 to 180 MPa and the strain to break from 550 to 900%. The improved mechanical properties for higher processing temperatures may reflect better cohesion between particles due to higher chain mobility providing increased interdiffusion. Above the T_g of PS, however, the two components macrophase separate, which is easily observed during the second heating cycle of the DSC, as the mixed state T_g totally disappears.

The effect of processing time on the mechanical properties of core−shell baroplastic materials was also studied. Samples of PBA_{49}/PS_{51} (BS10) were processed by compression molding for different times (from 15 s to 15 min) at 25 °C. Figure 14 shows modulus values from tensile tests for specimens subjected to an applied pressure of 34.5 MPa for different times. No significant differences in modulus or yield strength are seen between samples, despite the changes in morphology indicated by SANS (Figure 6) and DSC for a similar system with increased processing time. These results suggest that baroplastics can be molded in relatively short time periods, a significant potential advantage of this fabrication route over conventional thermoplastic processing.

The importance of pressure-enhanced mixing to the mechanical properties was investigated by comparing the PLMA/PS (LS1) control described in the previous section to BS3, having comparable acrylate molecular weight, hard to soft component ratio, and average particle size. While stress−strain measurements showed some difference in performance (Table 2), a more dramatic difference was revealed by tear strength measurements, as shown in Figure 15. In this measurement a trouser-type sample of each system was subjected to strain at a rate of 300 mm/min until it broke or reached the machine force limit. For $PLMA_{46}/PS_{54}$, the tear propagates in a series of catastrophic events after minimal stress is applied. By contrast, for PBA_{47}/PS_{53} (BS4) the tear never propagates—instead, the "legs" of the specimen stretch and begin to yield. This result highlights differences in the interphase regions of the two samples. PLMA/PS has a poor interphase between components that allows easy propagation of the tear between domains. For the PBA/PS system, enhanced intermixing due to pressure-induced miscibility provides a tougher interphase that resists tear propagation.[33,34]

The processing method is also found to have a significant effect on the mechanical properties of a tested specimen.[35] Curve a in Figure 16 shows a representative tensile test from a PBA_{51}/PS_{49} sample (BS11) that was processed by compression molding at 25 °C. Curve b in Figure 16 shows the same material

extruded at 25 °C using a piston mold with a square opening that forms a flat ribbon instead of a cylinder. This ribbon was cut to a dogbone similar to films obtained by compression molding. Although the modulus and the tensile strength are similar, there is a significant difference in the strain to break—900% for the compression-molded sample vs 200% for the extruded film. Further studies are required to fully understand the role of processing mechanism on mechanical properties. Multiple processing through the piston mold was performed at pressure of 175 MPa (an applied force of 22 kN) at room temperature. Curve c in Figure 16 shows the mechanical behavior for the same PBA_{51}/PS_{49} system (BS11) processed 10 times by extrusion. Here a substantial change in properties is seen compared with the original processed specimen. There is an increase in the modulus, from 37 to 78 MPa, and in the tensile strength, from 1.8 to 2.64 MPa, with a decrease in strain to break of about 100%. As described above, multiple extrusions through the piston mold resulted in chain scission of the large polyacrylate chains to roughly half their original molecular weight. The change in mechanical properties might be ascribed to a decrease in PBA molecular weight and an increase in interphase between PS and PBA domains.

Conclusions

The two-stage emulsion polymerization technique employed in this work provides a high degree of control over the composition, size, and structure of core−shell nanoparticles. The baroplastic core−shell particles synthesized by this route could be processed at reduced temperatures by compression molding and extrusion. The mechanical behavior of the processed materials is highly dependent on composition, particle size, and processing conditions, which can be tuned to obtain the desired behavior, from elastomeric materials comparable to commercial styrenic block copolymer TPEs to stronger, more rigid products.

Though low-temperature processing of core−shell baroplastics eliminates thermal degradation, chain scission of the soft component can occur upon recycling for molecular weights above 1×10^6 g/mol, potentially influencing the mechanical properties of the final product.

It must be noted that the flow and processing of core−shell nanoparticles comprising an un-cross-linked core and glassy shell is not confined to systems exhibiting pressure-induced miscibility. However, the resulting mechanical properties are importantly influenced by component miscibility. Pressure-enhanced mixing results in tougher products, presumably due to the enhanced interphase between the components.

Low-temperature processing of core−shell polymer nanoparticles is an alternative polymer processing paradigm that may provide an opportunity to manufacture and recycle plastic and rubber products with substantial energy savings through reduced heating and cooling requirements and shorter cycle times, while eliminating thermal degradation.

Acknowledgment. The authors gratefully acknowledge Dr. Rex Hjelm for his assistance with the neutron scattering measurements. This work was sponsored by the Lord Foundation, Lord Corporation, and the MR-SEC Program of the National Science Foundation under Award DMR-0213282. This work has benefited from the use of the Los Alamos Neutron Science Center at the Los Alamos National Laboratory. This facility is funded by the U.S. Department of Energy under Contract W-7405-ENG-36.

References and Notes

(1) Holden, G. In *Thermoplastic Elastomers*, 2nd ed.; Holden, G., et al., Eds.; Hanser: Cincinnati, OH, 1996; p 574.
(2) Rader, C. P. In *Handbook of Plastics, Elastomers and Composites*, 3rd ed.; Harper, C., Ed.; McGraw-Hill: New York, 1996; p 5.1.
(3) Freedonia Group Report "Thermoplastic Elastomers to 2007", Dec 2003.
(4) Gonzalez-Leon, J. A.; Acar, M. H.; Ryu, S.-W.; Ruzette, A.-V. G.; Mayes, A. M. *Nature (London)* **2003**, *426*, 424.
(5) Pollard, M.; Russell, T. P.; Ruzette, A. V.; Mayes, A. M.; Gallot, Y. *Macromolecules* **1998**, *31*, 6493.
(6) Ruzette, A.-V. G.; Banerjee, P.; Mayes, A. M.; Russell, T. P. *J. Chem. Phys.* **2001**, *114*, 8205.
(7) Ryu, D. Y.; Lee, D. J.; Kim, J. K.; Lavery, K. A.; Russell, T. P.; Han, Y. S.; Lee, C. H.; Thiyagarajan, P. *Phys. Rev. Lett.* **2003**, *90*, no. 235501.
(8) Ruzette, A.-V. G.; Mayes, A. M.; Pollard, M.; Russell, T. P.; Hammouda, B. *Macromolecules* **2003**, *36*, 3551.
(9) Lee, C.; Chen, Y.; Chiu, W. *J. Appl. Polym. Sci.* **1998**, *69*, 13.
(10) Schellenberg, C.; Tauer, K.; Antonietti, M. *Macromol. Symp.* **2000**, *151*, 465.
(11) Dos Santos, F. D.; Fabre, P.; Drujon, X.; Meunier, G.; Leibler, L. *J. Polym. Sci., Part B: Polym. Phys.* **2000**, *38*, 2989.
(12) Dos Santos, F. D.; Leibler, L. *J. Polym. Sci., Part B: Polym. Phys.* **2003**, *41*, 224.
(13) Cheng, S.; Chen, Y.; Chen, Z. *J. Appl. Polym. Sci.* **2002**, *85*, 1147.
(14) Nelliappan, V.; El-Aasser, M. S.; Klein, A.; Daniels, E. S.; Roberts, J. E.; Pearson, R. A. *J. Appl. Polym Sci.* **1997**, *65*, 581.
(15) Ha, J. W.; Park, I. J.; Lee, S. B.; Kim, D. K. *Macromolecules* **2002**, *35*, 6811.
(16) Qiu, J.; Charleux, B.; Matyajaszewski, K. *Prog. Polym. Sci.* **2001**, *26*, 2083.
(17) Britton, D. J.; Lovell, P. A.; Heatley, F.; Venkatesh, R. *Macromol. Symp.* **2001**, *175*, 95.
(18) Aguiar, A.; Gonzalez-Villegas, S.; Rabelero, M.; Medizabal, E.; Puig, J. E.; Dominguez, J. M.; Katime, I. *Macromolecules* **1999**, *32*, 6767.
(19) Stubbs, J. M.; Sundberg, D. C. *Polymer* **2005**, *46*, 1125.
(20) Song, M.; Hammiche, A.; Pollock, H. M.; Hourston, D. J.; Reading, M. *Polymer* **1995**, *36*, 3313.
(21) Hourston, D. J.; Song, M.; Hammiche, A.; Pollock, H. M.; Reading, M. *Polymer* **1997**, *38*, 1.
(22) Sundberg, D. C.; Durant, Y. G. *Polym. React. Eng.* **2003**, *11*, 379.
(23) Beckett, S. T.; Craig, M. A.; Gurney, R. J.; Ingleby, B. S.; Mackley, M. R.; Parsons, T. C. L. *Trans IChemE, Part C* **1994**, *72* 47.
(24) Flemings, M. C. *Metall. Trans. B* **1991**, *22*, 269.
(25) Morton-Jones, D. H. *Polymer Processing*; Chapman & Hall: London, 1989; pp 41−44.
(26) Buchholz, B. A.; Zahn, J. M.; Kenward, M.; Slater, G. W.; Barron, A. E. *Polymer* **2004**, *45*, 1223.
(27) Ballauf, M.; Wolf, B. A. *Macromolecules* **1981**, *14*, 654.
(28) Metzner, A. B.; Metzner, A. P. *Rheol. Acta* **1970**, *9*, 174.
(29) Merrill, E. W.; Leopairat, P. *Polym. Eng. Sci.* **1980**, *20*, 505.
(30) Lu, M.; Keskkula, H.; Paul, D. R. *Polymer* **1996**, *37*, 125.
(31) Gagnon, K. D.; Lenz, R. W.; Farris, R. J.; Fuller, R. C. *Rubber Chem. Technol.* **1992**, *65*, 761.
(32) Joseph, S.; Thomas, S. *Eur. Polym. J.* **2003**, *39*, 115.
(33) Ward, I. M.; Hadley, D. W. *An Introduction to the Mechanical Properties of Solid Polymers*; Wiley: New York, 1993; p 12.9.
(34) Ajji, A. In *Polymer Blends Handbook*; Utracki, L. A., Ed.; Kluwer: Dordrecht, 2002; Vol. 1, pp 4.1, 4.6.
(35) Dumoulin, M. M. In *Polymer Blends Handbook*; Utracki, L. A., Ed.; Kluwer: Dordrecht, 2002; Vol. 2, p 10.11.

MA0508045